Int. J. Heat Mass Transfer. Vol. 25, No. 5, pp. 603–614, 1982
Printed in Great Britain

0017 9310/82/050603 12 $03.00/0

HEAT TRANSFER FROM PIN-FINS SITUATED IN AN ONCOMING LONGITUDINAL FLOW WHICH TURNS TO CROSSFLOW

E. M. SPARROW and E. D. LARSON
Department of Mechanical Engineering, University of Minnesota, Minneapolis, MN 55455, U.S.A.

(*Received* 7 *August* 1981 *and in revised form* 8 *October* 1981)

Abstract—Experiments were performed to determine per-fin heat transfer coefficients for pin-fin arrays exposed to a novel airflow arrangement. The flow enters the array longitudinally but, owing to the blocking action of the fin base surface, is forced to turn and exit the array with a predominantly crossflow orientation. Geometric parameters varied during the experiments included the fin height to diameter ratio H/D and the inter-fin pitch to diameter ratio S/D. For each geometric configuration, the Reynolds number was varied over an order of magnitude. In general, fins situated adjacent to the edges of the array have higher heat transfer coefficients than those situated in the interior of the array. The Nusselt numbers for the edge-adjacent fins are virtually independent of H/D and S/D when they are correlated with a Reynolds number based on a crossflow velocity. For the interior fins, a Reynolds number based on a longitudinal flow velocity was used to achieve a correlation which was insentitive to H/D and S/D. The pressure drop across the array was measured and presented in dimensionless form relative to a specially defined velocity head which gave a universal pressure drop result for all operating conditions.

NOMENCLATURE

A, naphthalene surface area;
A_C, area for crossflow, equation (5);
A_L, area for longitudinal flow, equation (4);
D, pin-fin diameter;
$\mathscr{D}$, naphthalene–air diffusion coefficient;
H, height of fin;
K, mass transfer coefficient, equation (1);
L, side dimension of base plate;
$\dot{m}$, rate of mass transfer;
Nu, Nusselt number;
Pr, Prandtl number;
Δp, pressure drop across array;
Re_C, $= \rho V_C D/\mu$, crossflow Reynolds number;
Re_L, $= \rho V_L D/\mu$, longitudinal flow Reynolds number;
S, inter-fin center-to-center spacing;
Sc, Schmidt number;
Sh, $= KD/\mathscr{D}$, Sherwood number;
V_L, longitudinal velocity, equation (6);
V_C, crossflow velocity, equation (6);
V_*, reference velocity, equation (13);
$\dot{w}$, airflow rate.

Greek symbols

μ, viscosity of air;
ρ, density of air;
ρ_{nw}, naphthalene vapor density at fin surface;
ρ_{nb}, naphthalene vapor density in fluid bulk;
ν, kinematic viscosity of air.

INTRODUCTION

ENHANCEMENT techniques are frequently called for to assist in the dissipation of a given heat load and in attainment of thermal control. The attachment of fins (i.e. extended surfaces) to a primary heat transfer surface is a common approach to enhancement. A wide variety of finning arrangements is now in use and, among these, particular attention will be given here to pin-fins. A pin-fin is a cylinder attached perpendicular to a primary heat transfer surface and, in most applications, it is customary to use an array of pin-fins to attain the desired enhancement. In conventional practice, an airstream moves parallel to the primary heat transfer surface and passes in crossflow through the pin-fin array.

In the present paper, pin-fins exposed to a novel fluid flow arrangement will be considered, and the basic heat transfer and pressure drop characteristics of the system will be determined experimentally. The description of the flow configuration is facilitated by reference to Fig. 1. As seen in the upper diagram, the airflow approaches the array from the direction parallel to the axes of the cylinders. The air enters the array and begins to flow longitudinally through the inter-fin spaces until forced to turn by the blocking action of the base plate to which the fins are attached. Subsequent to turning, the flow exits the array in a direction that is more or less in crossflow to the cylinders. Thus, certain of the fins within the array experience predominantly longitudinal flow, while other fins experience predominantly crossflow.

A plan view of the pin-fin array is shown in the lower diagram of Fig. 1. The system consisted of a square base plate to which were attached 36 equally spaced pin-fins. The fin array and its base plate were situated in a large chamber. A square aperture of dimensions identical to that of the base plate was machined into the upper wall of the chamber, and the array was

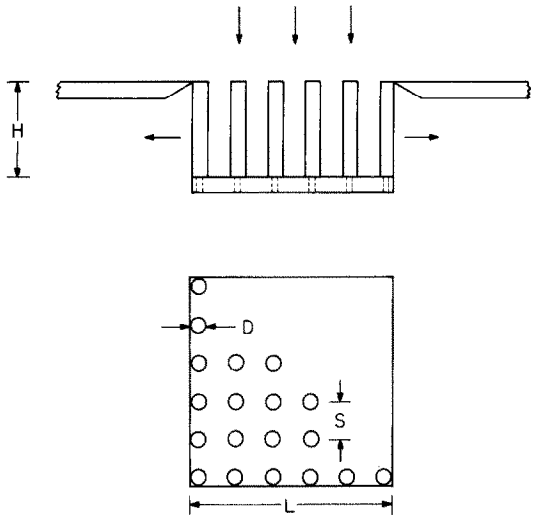

FIG. 1. Schematic of pin-fin array and airflow arrangement.

positioned so that the exposed tips of the fins were coplanar with the exterior surface of the wall (Fig. 1, upper diagram). In a given data run, air was drawn over the fins and the base plate by applying suction to the chamber.

The main objective of the work was to determine per-fin heat transfer coefficients at all positions in the array. These results were obtained as a function of the Reynolds number and of the relevant geometric parameters, to be described shortly. The heat transfer coefficients were measured through use of the naphthalene sublimation technique, whereby mass transfer data can be converted to heat transfer data using the well established analogy between the two processes. The results are presented here in terms of the dimensionless mass transfer coefficient, i.e. the Sherwood number. Pressure drop measurements across the fin array were also made and are presented here in dimensionless form by referencing the data to an appropriate velocity head.

The effect of two dimensionless geometric parameters on the heat transfer and pressure drop characteristics was studied. These parameters are the ratio H/D of the pin-fin height to the diameter and the ratio S/D of the pin-fin center-to-center spacing to the diameter. Three values of H/D were employed in the experiments, namely, 4, 8 and 12, while the selected nominal values of the S/D ratio were 2 and 4. For each of the six geometrical configurations, the Reynolds number was varied by an order of magnitude.

In view of the existence of the two types of flow (longitudinal and crossflow) in various parts of the array, the data are presented using two different definitions of the Reynolds number. One is based on the longitudinal flow velocity at the entrance plane of the array, while the other is based on the crossflow velocity at the exit plane of the fin array. Results for pin-fins situated along the outside edge of the array correlated well using the crossflow Reynolds number, while those situated in the interior of the array, away from the edges of the base plate, correlated well using the longitudinal flow Reynolds number. These correlations confirmed expectations, originally raised by supplementary oil–lampblack flow visualization studies, that the two types of flows did indeed exist in the pin-fin array.

In analyzing the measured pressure drops, it was found possible to construct a reference velocity so that the results for the dimensionless pressure loss are essentially independent of the Reynolds number and of the geometric parameters S/D and H/D.

A search of the literature revealed that no prior studies of the type described here have been performed. However, extensive literature exists for heat transfer from tube banks in crossflow and for tube bundles in longitudinal flow. In view of the two complementary correlations of the experimental data using different Reynolds numbers, comparisons of the present results with the aforementioned literature results for crossflow and longitudinal flow were attempted. It was found possible to make a meaningful comparison between the results for the edge-adjacent pin-fins and literature correlations for tube banks in crossflow. Unfortunately, the requisite information for the longitudinal flow case was not available in the literature, so that no comparison could be made.

EXPERIMENTAL APPARATUS

The pin-fin array and the test chamber which houses the array have already been mentioned in the Introduction, and the array is illustrated in Fig. 1. The relevant features of these components will now be elaborated, and the other parts of the apparatus will be described. To conserve space, it will be necessary to omit many details relating to apparatus fabrication, structure and dimensions, and to experimental technique. This information is available in [1] on which this paper is based.

Pin-fin array. The heart of the apparatus is the pin-fin array and its base plate, as pictured schematically in Fig. 1. Each fin is a circular cylinder machined with a shank of smaller diameter at its lower end to facilitate attachment to the base plate (see Fig. 1, upper diagram). There were two basic types of pin-fins used during the course of the experiments. One type had a coating of naphthalene on the surfaces of the fin that are exposed to the airflow (i.e. the cylindrical surface and the tip). The other type was a metallic cylinder. Both the naphthalene-coated cylinders and the metallic cylinders had the same finished dimensions. The fabrication of both types of cylinders will be described shortly.

In order to cover the desired range of geometrical parameters, cylinders of two different diameters were fabricated, with a different base plate for each diameter. Both base plates had a common side dimension L (= 7.684 cm) in order to fit the aperture in the upper wall of the test chamber. Furthermore, the same

number of pin-fins (= 36) were used to form the arrays for the two different diameters.

The larger of the fin diameters was 0.635 cm. For this diameter and with the side dimension L of the base plate equal to 7.684 cm, it is readily calculated that for a 36-fin array of the type shown in the lower diagram of Fig. 1, the center-to-center spacing S is 1.410 cm. This yields an S/D ratio of 2.22, which is an adequate approximation of the desired nominal value $S/D = 2$. The fins were first fabricated with a height $H = 12D$ (H is the fin height that is exposed to the airflow). Once the experiments for the H/D ratio were completed, the height was reduced to correspond to $H/D = 8$. When the data runs for $H/D = 8$ had been carried out, a further reduction in height was made so that runs for $H/D = 4$ could be made.

The smaller of the fin diameters was 0.357 cm, and the corresponding center-to-center distance was 1.465 cm, which yields an S/D ratio equal to 4.10 (approximating the nominal S/D value of 4.0). Again the fins were initially fabricated with a height $H = 12D$, and the height was successively reduced to $H/D = 8$ and to $H/D = 4$ as the experiments proceeded.

The larger diameter fins were cut from $\frac{1}{4}''$ dia. drill rod stock, while the smaller diameter fins were made from $\frac{9}{64}''$ drill rod. Drill rod was used to ensure uniformity of diameter among all 36 fins of each set. All fins were undercut at one end so as to provide a shank which mated with the base plate, as discussed earlier. Those fins that were not to participate in the naphthalene mass transfer process were finished so that the length of the main body of the fin (i.e. the length exposed to the airflow) was equal to $12D$.

To facilitate the coating of the pin fins for the mass transfer process, the main body of the fin was undercut by about $\frac{3}{4}$ mm on the diameter and was cut about $\frac{1}{2}$ mm shorter than the desired finished length. Following the undercutting operation, the resulting cylindrical surface was machined so as to form a screw thread. The purpose of the screw thread was to provide cavities to aid in the adhesion of the naphthalene. The pin-fins thus machined were dipped into a container of molten naphthalene, the dipping process being performed in many stages so that the surface temperature was kept low enough to avoid remelting of the naphthalene that had solidified on it. Once a sufficiently thick coating had been built up, the coated fin was machined in a lathe to remove the excess solidified naphthalene. The machining was carried on until the diameter of the naphthalene-coated fin was equal to the diameter of the uncoated fins. The tip of the coated fin was also machined so that its height H was identical to that of the other fins.

For efficiency in executing the experiments, it was standard practice to coat and machine at least 8–10 fins at a time. Once the coated fins had been fabricated, they were wrapped in impermeable plastic and placed in the laboratory where the experiments were to be conducted. Freshly prepared coated fins were employed for each data run (i.e. pin-fins were never reused). Subsequent to each data run, the remaining naphthalene coating was removed by melting and evaporation in preparation for the next round of coating and machining operations.

Test chamber. The function of the test chamber is to enable the experiments to be performed in the suction mode. The chamber is a large, vertical structure made of heavy-gage steel. It is 152 cm in height and has a 61 × 61 cm horizontal cross-section—its large size having been chosen to ensure that the walls of the chamber would not affect the flow pattern within the fin array.

The chamber is totally enclosed and airtight except for the aforementioned aperture in its upper wall (the perimeter of the aperture is identical to the perimeter of the array) and an air exhaust port in its lower wall. Figure 1 (upper diagram) shows the aperture with the fin array in place. The beveling of the wall adjacent to the aperture was performed to avoid possible interference with the turning of the flow. A removable window fitted to one of the side walls of the enclosure was used for viewing the array and for access to the interior of the chamber in order to align and position the array.

The array was supported from below by a vertical, rod-like structure which was threaded into the underside of the base plate of the array. In turn, the support structure was anchored to a horizontal length of angle iron which bridged between the walls of the chamber; the bridge was situated 36 cm below the base plate to avoid interference with the flow in the array.

The support structure was designed to enable precise positioning of the array in the aperture in the upper wall of the chamber, both with regard to vertical and transverse alignment. In addition, the structure could be rotated and depressed to facilitate the installation and removal of fins situated along the edges of the array. The installation and removal was accomplished from above, through the aperture in the upper wall. The edge-adjacent pin-fins were in such close proximity to the sides of the aperture that they could not be installed or removed unless the entire array were depressed and rotated.

Other apparatus components. To provide an overview of the apparatus, the flow circuit will now be traced. Air is drawn from the laboratory room into the aperture in the upper wall of the test chamber. The air passes through the fin array from which it exits into the chamber proper and flows downward through the chamber to a port at the bottom. From the exit port, the air is ducted to an air-handling system which includes, in parallel configuration, a pair of calibrated rotameters, two control valves, and a pair of blowers with a combined capacity of 130 cfm. The blowers were situated in a service corridor outside of the laboratory room, and their discharge was vented outdoors.

An essential feature in the determination of the mass transfer coefficients is the measurement of the mass of the naphthalene-coated fins before and after a data

run. This measurement was performed with a Sartorius analytical balance with a smallest scale division of 0.1 mg and a total capacity of 200 g. The temperature of the air entering the array was measured with an ASTM-certified thermometer with a smallest division of 0.1°F.

Pressure drop studies were also performed, and for this purpose three pressure taps were installed in the side walls of the test chamber. The pressure differences between these taps and the ambient were read with a Baratron solid-state, capacitance-type pressure meter capable of detecting differences as small as 10^{-4} mm Hg. Water manometers were used to measure the pressures at the rotameters, and the ambient pressure was measured with a laboratory-grade barometer.

Special tools were developed for installing (and removing) the naphthalene-coated fins in (from) the array. These tools enabled the fins to be handled without finger contact (which would have resulted in an unwanted temperature rise of the fin) and without damage to the naphthalene surface.

EXPERIMENTAL PROCEDURE

The objective of the research is to determine mass (heat) transfer coefficients at each pin-fin location, with the expectation that fin-to-fin variations would occur owing to differences in the nature of the fluid flow in different parts of the array. These local per-fin results are to be obtained for each of a large number of operating conditions parameterized by H/D, S/D and Re. In order to fulfil this objective with a feasible work effort, it was deemed realistic to employ only one mass transfer-participating pin-fin in the array during a given data run, with the other (metallic) fins being present to create the proper pattern of fluid flow.

This approach takes full account of the hydrodynamic interactions which occur in the array. Inter-fin mass (heat) transfer interactions are not accounted for, but these are expected to be of lesser importance than the hydrodynamic interactions. Furthermore, in any heat transfer application where the change in the bulk temperature of the air passing through the array is small relative to the fin-to-air temperature difference, the inter-fin thermal interactions will have a negligible effect on the results.

In the actual execution of the experiments, advantage was taken of the geometric symmetry of the array. If reference is made to the lower diagram of Fig. 1, it is seen that the entire array can be subdivided into geometrically identical octants. Visualization studies using the oil–lampblack technique affirmed that the patterns of fluid flow in all octants were, indeed, identical. Thus, by collecting data in any one octant, information is available for the entire array. In each such octant, there are six distinct pin-fin locations at which data have to be collected in order to provide complete information for the array as a whole.

In view of the aforementioned symmetry, it was possible to employ more than one active pin-fin for each run and still obtain results as if only one active fin were present. This was accomplished by placing an active fin in one or more of the symmetry octants of the array. At most, four fins were employed during a given data run, one in each of four octants.

Certain aspects of the experimental procedure were mentioned in the Apparatus section of the paper, and additional relevant features will now be described. A detailed step-by-step account of the experimental procedure is available in [1].

As noted earlier, the freshly cast and machined naphthalene-coated fins, individually wrapped in plastic, were placed in the laboratory prior to the initiation of a data run. To prepare for the data run, the room lighting and the blowers in the air-handling system were turned on at least 30 min before the intended start of the run, this period having been found suitable for the establishment of both steady temperatures in the room and steady flow in the apparatus. The steady temperature, once established, was maintained to within 0.05–0.1°C during the data run by the temperature control system for the room.

The next preparatory step involved the attainment of thermal equilibrium between the naphthalene-coated fins and the airflow passing through the array. The attainment of temperature equality is a necessary prerequisite for the evaluation of the naphthalene surface temperature from the measured air temperature. As will be seen shortly, the naphthalene surface temperature is used to evaluate the naphthalene vapor pressure (the vapor pressure is sensitive to temperature, varying by about 10% per °C). To attain the desired equilibrium, the naphthalene-coated fins, each jacketed in a close-fitting sealed Teflon sleeve to minimize extraneous sublimation, were inserted at pre-selected positions in the array. The pin-fins were allowed to remain in the array for about 30 min, during which time they were exposed to the airflow rate that had been set for the data run.

After the equilibration period, the fins were removed from the array, weighed on the analytical balance (with Teflon jackets removed), and then returned (with jackets in place) to the array for an additional 5–10 min equilibration period. This additional interval was allowed to dissipate possible temperature imbalances which might have occurred during the removal, weighing and reinstallation.

The mass transfer period was initiated by the removal of the Teflon jackets, thereby exposing the naphthalene-coated fins to the airflow. During the run, readings of temperature, flow rate, rotameter pressure and barometric pressure were taken at regular intervals. The duration of the run was chosen so that the average change of thickness of the naphthalene coating due to sublimation would be about 0.0025 cm. To terminate the run, the naphthalene-coated fins were jacketed, removed from the array, and weighed (with jackets removed).

At this point, a mock data run was carried out to determine a correction for any extraneous mass trans-

fer that may have occurred in the period between the first and second weighings. All of the steps that had been performed between the first and second weighings were repeated, except for the exposure to the airflow, and following this, a third weighing was made. The difference between the second and third weighings yielded a subtractive correction which was applied to the difference between the first and second weighings. The correction was on the order of 2% of the net mass transfer.

The pressures drop data were collected in runs made specifically for that purpose (i.e. without mass transfer). In a pressure run for a given geometrical configuration (i.e. given H/D and S/D), the flow rate was varied in small steps (about 15 steps over an order of magnitude change in flow rate) and, at each step, the three pressure taps in the plenum side wall were read with the Baratron pressure meter.

DATA REDUCTION

The procedures used to evaluate the per-fin mass transfer coefficient, its dimensionless counterpart, Sherwood number, and Reynolds number will now be described. The analogy between heat and mass transfer will then be employed to demonstrate how the Sherwood numbers for naphthalene sublimation can be transformed into Nusselt numbers for heat transfer. As the final item in the data reduction, dimensionless pressure loss coefficients will be evaluated.

If the corrected, per-fin change of mass during a data run is denoted by ΔM and τ is the duration of the run, then the rate of mass transfer $\dot{m}$ follows as $\Delta M/\tau$. The mass transfer coefficient K can then be evaluated from its definition

$$K = (\dot{m}/A)/(\rho_{nw} - \rho_{nb}). \quad (1)$$

In equation (1), A is the naphthalene surface area per fin, while ρ_{nw} and ρ_{nb} respectively denote the naphthalene vapor density at the surface of the fin and in the bulk flow.

There is a very slight change in the naphthalene surface area owing to the sublimation that takes place during a data run. Consequently, the area A in equation (1) was evaluated as the average of the initial and final areas. The vapor density ρ_{nw} at the surface was computed by a two-step process. First, the vapor pressure was found from the Sogin vapor pressure–temperature relation [2], and then the vapor density was obtained from the perfect gas law. For the conditions of the experiments, $\rho_{nb} = 0$.

The Sherwood number was defined using the diameter D of the pin-fin as the characteristic dimension, so that

$$Sh = KD/\mathscr{D} \quad (2)$$

where $\mathscr{D}$ is the mass diffusion coefficient. The latter can be eliminated by noting that the Schmidt number Sc, which is the mass transfer counterpart of the Prandtl number, is equal to $\nu/\mathscr{D}$ (ν = kinematic viscosity). Then, when Sc is introduced in (2),

$$Sh = (KD/\nu)Sc. \quad (3)$$

The Schmidt number for naphthalene diffusion in air is 2.5 [2]. Also, in view of the minute amounts of naphthalene vapor that were present, ν was evaluated for pure air.

With regard to the Reynolds number, it has already been noted in the Introduction that two complementary definitions, one for longitudinal flow and one for crossflow, will be used in the correlation of the results. Correspondingly, two cross-sectional areas for fluid flow will now be defined. One of these, the longitudinal flow area A_L, is equal to the free flow area encountered by the air as it enters the array. With reference to the lower diagram of Fig. 1, it follows that

$$A_L = L^2 - 36(\pi D^2/4) \quad (4)$$

where the number 36 represents the number of pin-fins in the array. The crossflow area A_C is evaluated as the minimum open area between the fins through which the air passes in crossflow as it exits from the array. With the aid of Fig. 1, A_C is expressible as

$$A_C = 4(L - 6D)H. \quad (5)$$

Velocities V_L and V_C then follow as

$$V_L = \dot{w}/\rho A_L, \quad V_C = \dot{w}/\rho A_C. \quad (6)$$

With these and with the diameter D used as the characteristic dimension, the Reynolds numbers Re_L and Re_C are:

$$Re_L = \rho V_L D/\mu = \dot{w}D/\mu A_L, \quad (7)$$

$$Re_C = \rho V_C D/\mu = \dot{w}D/\mu A_C. \quad (8)$$

With regard to the analogy between heat and mass transfer, the Nusselt and Sherwood numbers are generally expressed in the functional forms

$$Nu = f(Re, Pr), \quad Sh = f(Re, Sc) \quad (9)$$

where the function f is the same for both heat and mass transfer. For the correlation of experimental data, it is common to seek power law representations

$$Nu = CRe^m Pr^n, \quad Sh = CRe^m Sc^n \quad (10)$$

where, again, by the analogy, the quantities C, m and n are common to both heat and mass transfer. From equation (10), it follows that at a given Reynolds number

$$Nu = (Pr/Sc)^n Sh. \quad (11)$$

The exponent n is commonly taken to be 1/3, but the recent correlation of tube bank data by Zukauskas [3] gives rise to an n value of 0.36. If the latter is employed, then the Sherwood numbers for naphthalene sublimation ($Sc = 2.5$) can be transformed to Nusselt numbers for heat transfer in air ($Pr = 0.7$) by the relation

$$Nu = 0.632Sh. \quad (12)$$

If the 1/3 power had been employed instead of 0.36, the constant 0.632 would be replaced by 0.654 (a

difference of about 3.4%). Thus, equation (12) enables the results of the present experiments to be applied to heat transfer between pin-fins and an airstream.

For a given geometrical configuration, the measured pressure drop Δp at each Reynolds number was made dimensionless by using the velocity head $\frac{1}{2}\rho V_L^2$ as a reference quantity. It was then observed that $\Delta p/\frac{1}{2}\rho V_L^2$ was quite insensitive to variations in the Reynolds number. Therefore, a single value of $\Delta p/\frac{1}{2}\rho V_L^2$ can be employed to express the pressure drop characteristics for each geometrical configuration. However, $\Delta p/\frac{1}{2}\rho V_L^2$ was found to vary from configuration to configuration, as did $\Delta p/\frac{1}{2}\rho V_C^2$.

A reference velocity V_* was sought so that $\Delta p/\frac{1}{2}\rho V_*^2$ would have virtually the same value for all the investigated configurations. This objective is fulfilled when V_* is evaluated as

$$V_* = (V_L^2 + V_C^2)^{1/2}. \tag{13}$$

Thus, in terms of $\Delta p/\frac{1}{2}\rho V_*^2$, all the experimental results can be reported in terms of a single number.

RESULTS AND DISCUSSION

The presentation of mass (heat) transfer results will be structured to highlight the effects of each of the geometrical parameters, namely, pin-fin location in the array, fin height and fin spacing. Graphical presentations respectively focused on these parameters are made in the first three parts of this section, where the Reynolds number effect will also be displayed. With the insights gained from these graphs and their interpretations, the results are brought together in ways that facilitate their correlation, and the correlating equations are derived and stated. Comparisons with the literature are also made. The last part of the section deals with the pressure drop results.

Effect of pin-fin location

All of the Sherwood number data collected during the experiments are presented in Figs. 2 and 3, which respectively correspond to (nominal) inter-fin spacings, S/D, of 2 and 4. Although these figures cover all the parametric dependences of the data, they are most useful in identifying the effect of fin location on the Sherwood number, and they also show the trends with Reynolds number. Subsequent figures, differently structured, will be more suitable for identifying the effects of H/D and S/D.

Each of Figs. 2 and 3 is subdivided into three graphs, with each graph conveying Sh vs Re_L data for a specific dimensionless fin height H/D. The respective graphs, designated as (a), (b) and (c) (lower, middle and upper graphs), correspond to $H/D = 4, 8$ and 12. Within each graph, Sh vs Re data for six fin locations are plotted. The symbol designations for these positions are listed at the upper left of each figure, while a sketch of a typical quadrant of the array is included at the lower right to illustrate the positions of fins 1–6 (the cross designates the center of the array). From an examination of the sketch, it is evident that, because of symmetry, a knowledge of the Sherwood numbers at positions 1–6 is tantamount to knowing the Sherwood numbers at all 36 pin-fin positions in the array.

Throughout the discussion of results, fins 1–3 will be referred to as the edge-adjacent or exterior fins, while fins 4–6 will be called the interior fins. In anticipation of the tendency of certain data to group together, related data symbols have been used for those cases. Thus, upright and inverted triangles have been used to

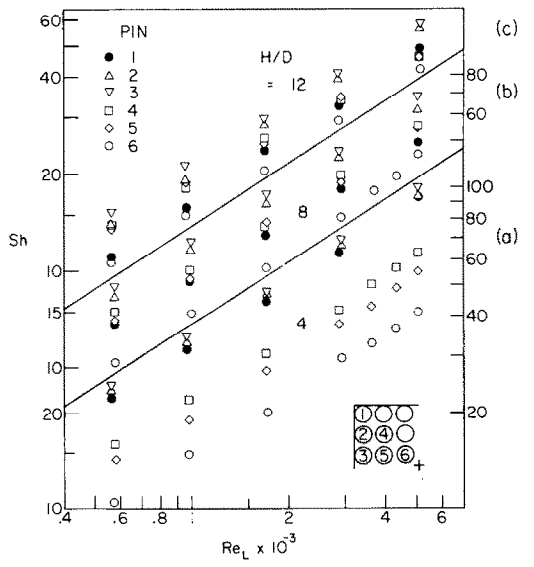

FIG. 2. Sherwood number presentation focused on the effects of fin location; $S/D = 2$.

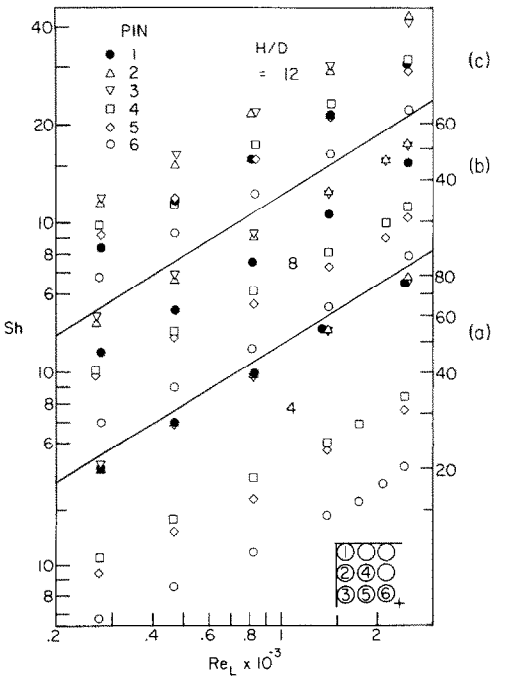

FIG. 3. Sherwood number presentation focused on the effects of fin location; $S/D = 4$.

represent the data for positions 2 and 3, while a square and a diamond (i.e. a rotated square) are used for positions 4 and 5.

It should be noted that the longitudinal flow Reynolds number Re_L has been used as the abscissa variable in Figs. 2 and 3. Since these figures are focused on the fin-to-fin Sherwood number variations for a given geometry (i.e. given H/D and S/D) and given airflow rate, either Re_L or Re_C are equally suitable abscissas (in fact, for a given H/D, S/D, and flowrate, Re_C is a simple multiple of Re_L).

From an overall examination of Figs. 2 and 3, it is seen that aside from the maverick behavior of the corner fin (pin-fin 1), there is a definite ordering of the Sherwood number with fin location. In general, fins situated in the interior of the array have lower Sherwood numbers than those situated adjacent to the edge. The lowest Sherwood numbers occur at fin location 6, which is the location closest to the center of the array. Fin locations 4 and 5 display higher Sherwood numbers than those at location 6, while the Sherwood numbers at locations 2 and 3 are still higher.

The figures also indicate how the aforementioned interior-to-exterior variation of the Sherwood number is affected by the fin height and by the inter-fin spacing. In light of the spreading of the data with decreasing H/D, it is clear that the spatial variations increase as the fin height decreases. Furthermore, comparison of Figs. 2 and 3 shows that greater spatial variations occur for larger inter-fin spacings.

Another consistent behavior which is in evidence in the figures is the close agreement between the Sherwood numbers for the fins at locations 4 and 5. This is not unexpected, since these locations are near neighbors and have approximately the same status with regard to interior–exterior positioning. This same grouping tendency is displayed by the fins at locations 2 and 3, and for the same reason.

The behavior of the fin at location 1 (the corner) is quite irregular. The Sherwood numbers at this location tend to be relatively low for the tallest fins. With decreasing fin height, the corner-fin Sherwood number tends to approach those of the edge-adjacent fins.

As expected, the Sherwood number increases with increasing Reynolds number. For given values of H/D and S/D, the data at any fin location appear to be reasonably well represented by a straight line. A more detailed examination of the Reynolds number dependence of the data will be deferred until later, when the two Reynolds numbers Re_L and Re_C will be employed to obtain tighter correlations than could be achieved with either of the Reynolds numbers alone.

Effect of H/D

Figures 4–7 have been prepared to identify and correlate the effect of fin height (i.e. H/D) on the Sherwood number. Among these four figures, 4 and 5 convey results for $S/D = 2$, with the data for the edge-adjacent fins 1–3 appearing in Fig. 4 and the data for the interior fins 4–6 in Fig. 5. Figures 6 and 7 are for $S/D = 4$, respectively providing results for fins 1–3 and for fins 4–6.

In each figure, there are two graphs which show the same data presented in different ways. In particular, in part (a) of each figure the Sherwood number is plotted as a function of the longitudinal Reynolds number Re_L, while in part (b) the same Sherwood number data are plotted against the crossflow Reynolds number Re_C. In order to separate the data for the respective fin locations, the Sherwood number itself is plotted for one location, $\frac{1}{2}Sh$ is plotted for the second location, and $\frac{1}{4}Sh$ is plotted for the third location. For each location, data are presented for all of the investigated values of H/D, and the corresponding symbol designations are given at the upper left of each figure. In addition, the fin layout is shown at the lower right.

From an examination of any one of Figs. 4–7, a remarkable difference between the right-hand and left-hand graphs is evident. In one of the graphs, the data for any fin location are virtually independent of H/D, while in the other graph there is a marked dependence upon H/D. An overall inspection of Figs. 4–7 shows that the H/D-independent correlation of the data for the edge-adjacent fins (1–3) occurs when the crossflow Reynolds number Re_C is used as the abscissa variable. On the other hand, for the interior fins (4–6), the H/D-independent correlation is achieved with the longitudinal flow Reynolds number Re_L on the abscissa.

The aforementioned tendency of the interior fin data to correlate with Re_L and the exterior fin data to correlate with Re_C can be readily rationalized. As noted in the Introduction, the airflow which enters the array is predominantly longitudinal while the flow which exits the array is predominantly in crossflow. This pattern was confirmed by oil–lampblack flow visualization, which also indicated the presence of an impingement zone centered on the base surface. From this, it follows that the interior fins 4–6 experience a predominantly longitudinal flow, while the exterior fins 1–3 experience a predominantly crossflow. It follows further, then, that the Sherwood number data for fins 4–6 should correlate better with the longitudinal flow Reynolds number, Re_L, while the data for fins 1–3 correlate more tightly using the crossflow Reynolds number, Re_C.

Effect of S/D

To explore the effect of S/D, the Sherwood number results for $S/D = 2$ and 4 were plotted together as a function of Reynolds number at a specific fin position and for a given H/D. For the exterior fin locations 1–3, it was found that Sh was relatively insensitive to S/D when the crossflow Reynolds number Re_C was used as the plotting parameter, while greater sensitivity to S/D was in evidence when the data were plotted against the longitudinal flow Reynolds number Re_L. On the other hand, for the interior fins 4–6, insensitivity to S/D was achieved with Re_L as the plotting variable.

Figure 8 presents the interior fin results plotted against Re_L and the exterior fin results plotted against

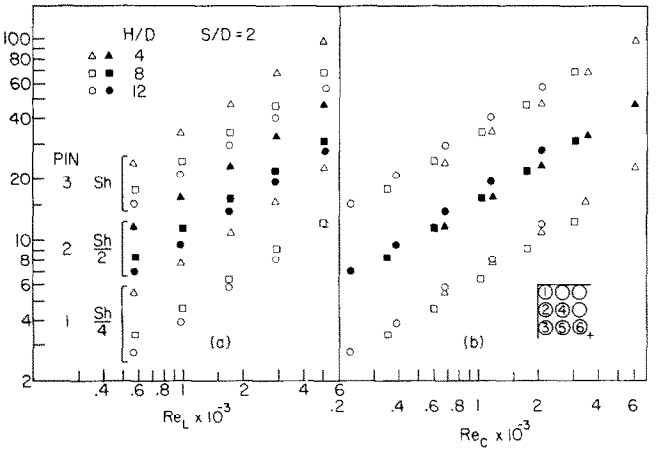

FIG. 4. Sherwood number presentation focused on the effects of H/D; fin locations 1–3 for $S/D = 2$.

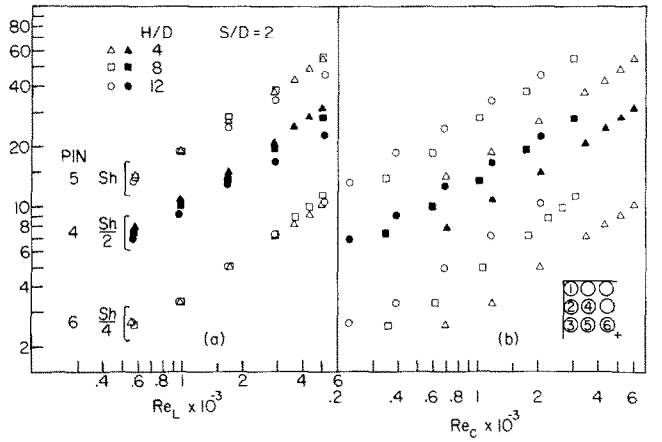

FIG. 5. Sherwood number presentation focused on the effects of H/D; fin locations 4–6 for $S/D = 2$.

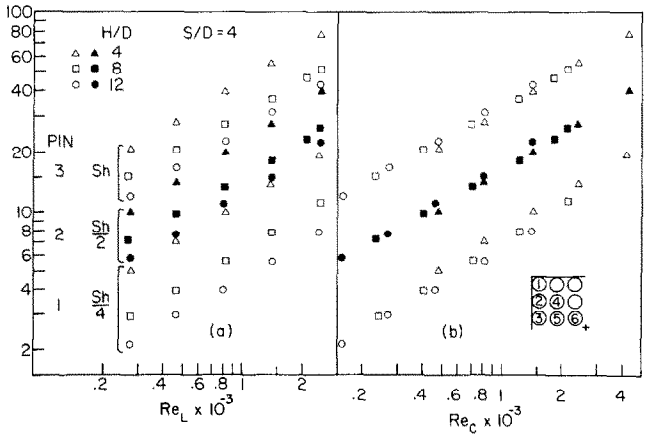

FIG. 6. Sherwood number presentation focused on the effects of H/D; fin locations 1–3 for $S/D = 4$.

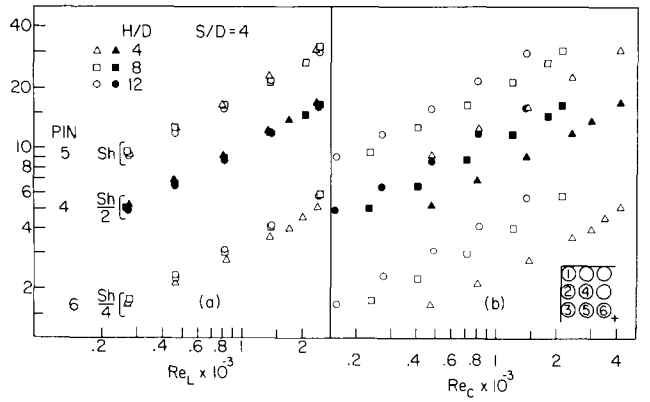

FIG. 7. Sherwood number presentation focused on the effects of H/D; fin locations 4–6 for $S/D = 4$.

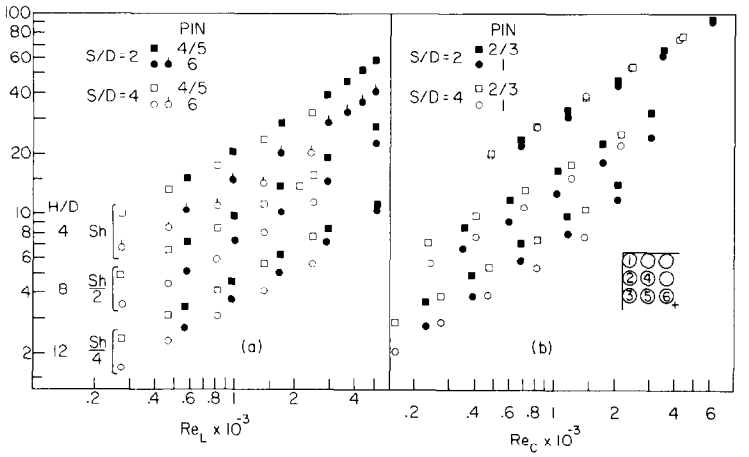

FIG. 8. Sherwood number presentation focused on the effects of S/D.

Re_C, respectively in the left-hand and right-hand graphs. For clarity, the data for the respective H/D have been separated by plotting Sh, $\frac{1}{2}Sh$ and $\frac{1}{4}Sh$, respectively for $H/D = 4, 8$ and 12. For each H/D, data for both $S/D = 2$ and 4 were plotted for each of the fin locations. For compactness, the data for locations 4 and 5 were averaged, and the average has been plotted as 4/5; similarly, the averaged data for locations 2 and 3 have been plotted as 2/3. As noted earlier, the data at 4 and 5 are in close agreement, as are the data at 2 and 3. In the figure, the $S/D = 2$ data are designated with blackened symbols, while those for $S/D = 4$ are represented by open symbols.

Inspection of Fig. 8 affirms the general insensitivity to S/D when the appropriate Reynolds numbers are employed as plotting variables. The rationale for this insensitivity is the same as that discussed earlier with regard to the H/D insensitivity.

Correlations and comparisons

The foregoing presentation has suggested Sherwood–Reynolds correlations which are insensitive to H/D and S/D. In Fig. 9, the exterior fin Sherwood numbers are plotted against Re_C. The lower graph shows results for fin locations 2 and 3, plotted together, while the upper graph is for the corner fin, 1. Least squares power law correlations for these data, shown as solid lines in the graph, are:

$$Sh = 0.321 Re_C^{0.647}, \quad (14)$$

$$Sh = 0.609 Re_C^{0.579}, \quad (15)$$

respectively for fin location 1 and for locations 2 and 3. The Sherwood number results given by equations (14) and (15) can be applied to compute heat transfer coefficients for airflow by transforming Sh to Nu in accordance with equation (12).

That the correlating equations (14) and (15) have

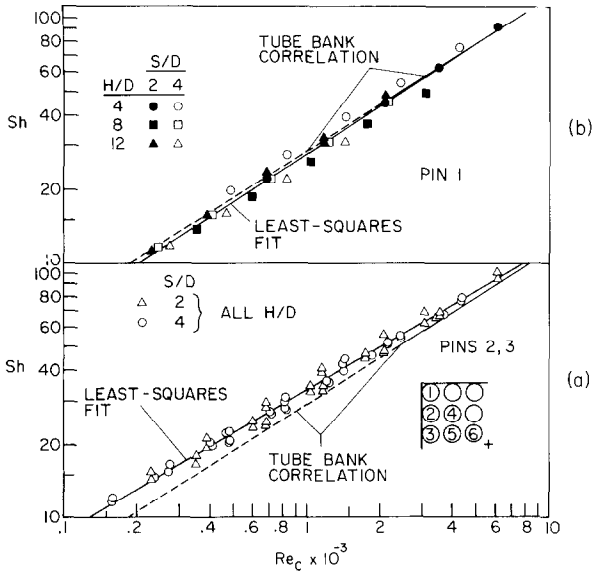

FIG. 9. Correlation of the Sherwood number for the edge-adjacent pin-fins.

different slopes is not surprising since the flow pattern adjacent to the corner fin is not the same as that adjacent to the other exterior fins. Although the Sherwood numbers from these equations deviate by about 25% at $Re_C = 300$, the deviation is only 5% at $Re_C = 6000$.

Comparison with the literature will now be considered and, for this purpose, the widely quoted tube-bank correlation of Grimison [4] for crossflow through an in-line, square array with $S/D = 2.22$ will be used. Grimison's results were for heat transfer in air ($Pr = 0.7$), and it has become conventional to scale his correlation to other Prandtl (or Schmidt) numbers by a $Pr^{1/3}$ (or $Sc^{1/3}$) factor [5]; this scaling was employed here. Another issue to be considered in employing the Grimison correlation relates to the correction factors [6] which account for the increase of the turbulence level as the flow develops from row to row. In the present experiments, high turbulence levels are expected at the edge-adjacent pin-fin locations as a result of the turning of the flow and of the fin-to-fin interactions. Consequently, Grimison's fully developed results (without a correction factor) will be used here.

For the aforementioned conditions, the Grimison correlation becomes

$$Sh = 0.385 Re_C^{0.625}. \tag{16}$$

In view of the specification [4] that the Grimison correlation applies for $Re_C \geq 2000$, only for that range has equation (16) been plotted as a solid line in Fig. 9. The equation has been extrapolated to lower Reynolds numbers as a dashed line in the figure.

The upper graph of Fig. 9 shows that equation (16) is remarkably close to the least squares fit of the data for the corner fin 1. In the lower graph, the equation deviates moderately from the data, especially at the lower Reynolds numbers. The observed deviations between the tube-bank correlation and the present data are not unexpected since the flow passing between the edge-adjacent fins is not strictly a crossflow. Although crossflow predominates, there is a residual longitudinal component which may enhance the mass transfer. The corner fin experiences a different and more complex flow pattern than the other edge-adjacent fins, thereby making it difficult to rationalize the excellent agreement between equation (16) and the data. Overall, considering the complexity of the flow field which prevails in the present configuration, the proximity of the tube-bank correlation to the external fin data of Fig. 9 has to be regarded as remarkable.

The Sherwood number data for the internal pin-fin locations 4–6 are brought together in Fig. 10, where they are plotted as a function of the longitudinal flow Reynolds number Re_L. Since the data for locations 4 and 5 are interleaved, they have been fit with a common least squares power law:

$$Sh = 0.357 Re_L^{0.582}. \tag{17}$$

As noted earlier, the data for location 6 (nearest the center of the array) are the lowest of all, and they have been fit to a separate least squares line

$$Sh = 0.190 Re_L^{0.626}. \tag{18}$$

The deviation between equations (17) and (18) is about 30%.

A thorough serach of the extensive literature on longitudinal flow in rod bundles failed to yield results suitable for comparison with the present data. In general, the published work was primarily confined to S/D ratios considerably less than 2 and to the fully developed regime.

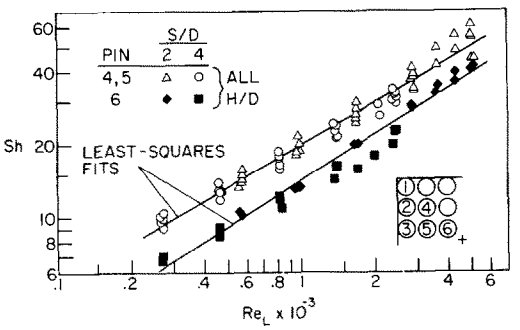

FIG. 10. Correlation of the Sherwood number for the interior pin-fins.

Pressure drop

The pressure drop across the array was made dimensionless by the velocity head $\frac{1}{2}\rho V_*^2$, where V_* is defined by equation (13). As noted earlier, $\Delta p/\frac{1}{2}\rho V_*^2$ was found to be insensitive to the Reynolds number for a given geometrical configuration. For $S/D = 2$, the values of $\Delta p/\frac{1}{2}\rho V_*^2$ corresponding to $H/D = 4, 8$ and 12 were 1.92, 1.98 and 2.04, while those for $S/D = 4$ were 2.17, 2.21 and 2.23. If the small variation with H/D is averaged out, then $\Delta p/\frac{1}{2}\rho V_*^2 = 1.98$ and 2.20 respectively for $S/D = 2$ and 4. Since these two numbers are not very different, it may be convenient, for design purposes, to report a single average value, namely, $\Delta p/\frac{1}{2}\rho V_*^2 = 2.09$.

CONCLUDING REMARKS

In this paper, basic heat (mass) transfer and pressure drop results have been reported for pin-fins exposed to a novel fluid flow arrangement. Heat transfer coefficients for each fin in the array were determined for parametric values of the geometry-related ratios H/D and S/D and of the Reynolds number.

In general, fins situated adjacent to the edges of the array have higher heat transfer coefficients than those situated in the interior of the array. It was found that the dimensionless transfer coefficients for the edge-adjacent fins could be rendered more or less independent of H/D and S/D if they were correlated with the crossflow Reynolds number Re_C. Similarly, the dimensionless coefficients for the interior fins were insensitive to H/D and S/D when correlated with the longitudinal flow Reynolds number Re_L. These findings are consistent with a physical picture whereby the interior fins are washed by a predominantly longitudinal flow and the edge-adjacent fins are washed by a predominantly crossflow.

The correlations are given by equations (14), (15), (17) and (18). The Sherwood numbers obtained from these equations can be used to calculate heat transfer coefficients for airflow by making use of the Nusselt–Sherwood relation of equation (12).

The pressure drop Δp across the array was made dimensionless by the velocity head $\frac{1}{2}\rho V_*^2$, where V_* is defined by equation (13). The use of V_* as a reference velocity more or less eliminates the effects of H/D and S/D on the dimensionless loss coefficient $\Delta p/\frac{1}{2}\rho V_*^2$, so that a single value $\Delta p/\frac{1}{2}\rho V_*^2 = 2.09$ may be used for design purposes.

REFERENCES

1. E. D. Larson, Heat transfer from pin fins situated in an oncoming longitudinal flow which turns to crossflow, M.S. Thesis, Dept. of Mechanical Engineering, University of Minnesota, Minneapolis, Minnesota (1981).
2. H. H. Sogin, Sublimation from disks to air streams flowing normal to their surfaces, *Trans. ASME* **80**, 61–71 (1958).
3. A. A. Zukauskas, Heat transfer from tubes in crossflow. In *Advances in Heat Transfer*, Vol. 8. Academic Press, New York (1972).
4. E. D. Grimison, Correlation and utilization of new data on flow resistance and heat transfer for cross flow of gases over tube banks, *Trans. ASME* **59**, 583–594 (1937).
5. F. P. Incropera and D. P. DeWitt, *Fundamentals of Heat Transfer*, p. 355. Wiley, New York (1981).
6. W. M. Kays and R. K. Lo, Basic heat transfer and flow friction data for gas flow normal to banks of staggered tubes, Stanford University Tech. Rep. No. 15 (1952).

TRANSFERT THERMIQUE A DES AIGUILLES SITUEES DANS UN ECOULEMENT ENTRANT LONGITUDINALEMENT POUR DEVENIR UN COURANT CROISE

Résumé—Des expériences sont conduites pour déterminer les coefficients de transfert par aiguille pour un arrangement exposé à un écoulement d'air frais. L'écoulement pénètre longitudinalement mais, sous l'effet de blocage par la surface de base des ailettes, il est obligé de tourner et il sort avec une orientation prédominante de courant croisé. Des paramètres géométriques sont variables dans les expérimentations comme le rapport H/D, hauteur/diamètre des aiguilles, et le pas entre aiguilles rapporté au diamètre S/D. Pour chaque configuration géométrique, le nombre de Reynolds est variable. En général, les aiguilles proches de l'entrée ont les coefficients de transfert plus élevés que celles situées au coeur de l'arrangement. Le nombre de Nusselt relatif aux premières est virtuellement indépendant de H/D et S/D quand il est exprimé en fonction d'un nombre de Reynolds basé sur une vitesse de courant croisé. Pour les aiguilles à l'intérieur, un nombre de Reynolds basé sur une vitesse d'écoulement longitudinal est utilisé pour établir une formule qui fait intervenir H/D et S/D. La perte de charge à travers l'arrangement est mesurée et présentée sous une forme adimensionnelle à partir d'une vitesse particulière qui donne une perte de pression universelle valable pour toutes les conditions expérimentales.

WÄRMEÜBERGANG AN NADELRIPPEN BEI ANSTRÖMUNG IN LÄNGSRICHTUNG MIT ÜBERGANG IN KREUZSTROM

Zusammenfassung—Es wurden Experimente zur Bestimmung der Einzelwärmeübergangskoeffizienten für Anordnungen von Nadelrippen in einer neuartigen Luftströmungsart durchgeführt. Die Strömung tritt in Längsrichtung der Nadeln in das Rippenpaket ein, wird jedoch durch die Blockierungswirkung der Grundfläche zur Richtungsänderung gezwungen und verläßt die Rippenanordnung vorwiegend im Kreuzstrom. Die im Verlauf der Experimente variierten geometrischen Parameter waren das Verhältnis von Rippenhöhe zu Durchmesser H/D und das Verhältnis von Rippenabstand zu Durchmesser S/D. Für jede geometrische Konfiguration wurde die Reynolds-Zahl über eine Größenordnung variiert. Im allgemeinen haben die Rippen an der Außenseite des Pakets höhere Wärmeübergangskoeffizienten als im Innern. Die Nusselt-Zahlen der außenliegenden Rippen sind praktisch unabhängig von H/D und S/D, wenn sie in Abhängigkeit von einer mit der Kreuzstromgeschwindigkeit gebildeten Reynolds-Zahl dargestellt werden. Für die innenliegenden Rippen wurde eine mit der Längsstromgeschwindigkeit gebildete Reynolds-Zahl zur Korrelation verwendet, wobei sich eine starke Abhängigkeit von H/D und S/D ergab. Der Druckabfall im Rippenpaket wurde gemessen und in dimensionsloser Form, bezogen auf den Staudruck einer besonders definierten Geschwindigkeit, dargestellt, woraus sich ein allgemeingültiges Ergebnis für alle Betriebsbedingungen ergab.

ТЕПЛОПЕРЕНОС ОТ ИГОЛЬЧАТЫХ РЕБЕР, ОБТЕКАЕМЫХ НАБЕГАЮЩИМ ПРОДОЛЬНЫМ ПЕРЕХОДЯЩЕМ В ПОПЕРЕЧНЫЙ ПОТОКОМ

Аннотация — Проведено экспериментальное определение коэффициентов теплопереноса для каждого из расположенных в пучке игольчатых ребер, обтекаемых потоком. Поток поступает в пучок в продольном направлении, но в силу блокирующего действия поверхности основания ребер совершает поворот и выходит из пучка практически в поперечном направлении. Эксперименты проводились с пучками различных геометрических конфигураций и с различными отношениями высоты ребра к диаметру, H/D, и шага ребер к диаметру, S/D. Для каждого варианта значение числа Рейнольдса отличалось на порядок величины. В общем случае для ребер, расположенных ближе к краям пучка, коэффициенты теплопереноса выше, чем в центре. Значения числа Нуссельта для ребер по краям пучка, как правило, не зависят от H/D и S/D в том случае, если они описываются числом Рейнольдса, отнесенным к скорости поперечного потока. Для ребер в центре пучка на основании числа Рейнольдса, отнесенного к скорости продольного потока, выведено обобщенное соотношение, не учитывающее влияние H/D и S/D. Проведено измерение перепадов давления поперек пучка, и результаты представлены в безразмерном виде как их отношение к специально замеряемому скоростному напору, с помощью которого можно определять перепады давления при всех рабочих условиях.